GDCh Research Article Angewandte International Edition Chemie www.angewandte.org

How to cite: Angew. Chem. Int. Ed. 2025, e202421448
doi.org/10.1002/anie.202421448

Proximity Labeling

# Two-Level Spatially Localized Proximity Labeling for Cross-Biological-Hierarchy Measurement and Manipulation

*Liusheng Chen, Yiran Li, Yuna Guo, Guyu Wang, Nan Feng, Jiahui Sun, Yihong Zhong, Yunyan Yao, Lin Ding,* and Huangxian Ju*

**Abstract:** Proximity labeling (PL) has emerged as a powerful technique for the in situ elucidation of biomolecular interaction networks. However, PL methods generally rely on single-biological-hierarchy control of spatial localization at the labeling site, which limits their application in multi-tiered biological systems. Here, we introduced another enzymatic reaction upstream of an enzyme-based PL reaction and targeted the two enzymes to markers indicating different biological hierarchies, establishing a two-level spatially localized proximity labeling ($P^2L$) platform for in situ molecular measurement and manipulation. Using the *cellular-* and *glycan-level* as the hierarchical models, we demonstrated the ability of $P^2L$ to efficiently execute a two-step logic operation and to discriminate target cells with different levels of glycosylation within mixed cell populations. By mounting clickable handles via $P^2L$, we reprogrammed the robust covalent assembly of cells at designated sites. The combination of $P^2L$ with proteomics led to the profiling of the protein microenvironment of specific glycans on target cells, revealing changes in tumor-cell-surface interactions under immune pressure from a glycan perspective. $P^2L$ provides not only a solution for revealing the heterogeneity of biological systems, but also new insights in the fields of intelligent logic computation, enzyme engineering, tissue engineering, etc.

## Introduction

In biological systems, the spatial organization of biomolecules dictates their interactions.[1] Elucidation of the sophisticated interaction networks is essential for understanding physiological processes.[2] The emerging proximity labeling (PL) technology utilizes genetic engineering or recognition molecules (such as antibodies, aptamers, or ligands) to direct a catalyst (enzymes[3] or photocatalysts[4]) towards the target molecules, thereby catalyzing the covalent conjugation of substrates to reactive groups in the localized environment, allowing for the in situ acquisition of information about proximal biomolecules (proteins, DNA, RNA, etc.). Peroxidases, such as horseradish peroxidase (HRP)[5] and enhanced ascorbate peroxidase 2 (APEX2),[6] are among the most extensively utilized biocatalysts for PL due to their remarkable labeling efficiency. Once localized to the target area, these enzymes can catalyze the conversion of phenol derivatives into phenoxy radicals in the presence of hydrogen peroxide ($H_2O_2$), which can form covalent adducts with electron-rich amino acid residues (tyrosine, etc.) of proximal proteins.[7] For example, these enzymes have been utilized to map the endogenous cell membrane interactome of the glucagon-like peptide-1 receptor[8] and to quantify phagosome proteomes during host-microorganism interactions.[9]

Generally speaking, life exists in a spatially organized form at levels ranging from biomolecules to cells, tissues, and whole organisms through consuming energy.[10] The high level of complexity, dynamics and fragility of biological systems can only be accurately reflected when analyzed in a comprehensive biological context. Therefore, the development of analytical techniques capable of spatial localization across biological hierarchies is expected to substantially enhance biological discovery and advance therapeutic interventions.

For PL technologies, the labeling region depends on the spatial localization of catalysts by gene expression or recognition orientation. Most of the current methods, especially those based on recognition, are unable to localize across hierarchical levels and only detect a collection of molecules/cells in the vicinity of a target molecule/cell. Furthermore, PL-generated tags are predominantly utilized for molecular information profiling, but their potential applications in cell tracking and engineering have been largely underestimated. Therefore, we believe that there is a need to superimpose additional levels of spatial selectivity on existing PL technologies to enable cross-level localization for biological measurement and manipulation (Scheme 1A).

[*] L. Chen, Dr. Y. Li, G. Wang, Dr. N. Feng, J. Sun, Y. Yao, Prof. L. Ding, Prof. H. Ju
State Key Laboratory of Analytical Chemistry for Life Science, School of Chemistry and Chemical Engineering, Nanjing University, Nanjing 210023, China
E-mail: dinglin@nju.edu.cn

Dr. Y. Guo
School of Clinical and Basic Medical Sciences, Shandong First Medical University, Jinan 250117, China

Dr. Y. Zhong
College of Chemistry and Materials, Jiangxi Normal University, Nanchang 330022, China

Prof. L. Ding
Chemistry and Biomedicine Innovation Center (ChemBIC), ChemBioMed Interdisciplinary Research Center, Nanjing University, Nanjing 210023, China

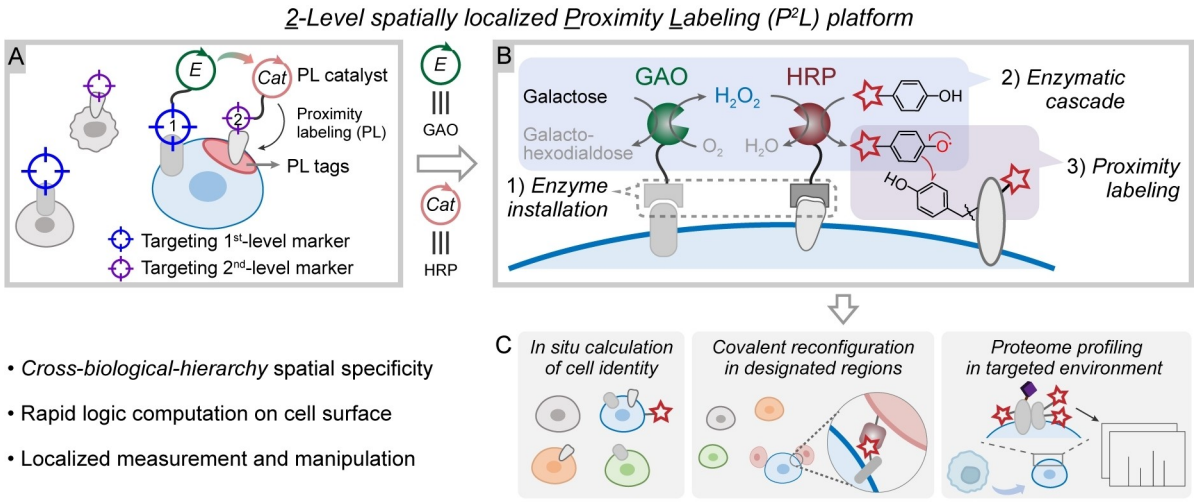


***Scheme 1.*** Design of the two-level spatially localized proximity labeling ($P^2L$) platform. (A) Principle of $P^2L$. An enzymatic reaction (the enzyme is labeled as *E*) can be introduced upstream of a catalysis-based proximity labeling (PL) reaction. Anchoring the two enzymes to the markers of different biological hierarchies leads to the establishment of the $P^2L$ platform. (B) Galactose oxidase (GAO) is incorporated as a switch for horseradish peroxidase (HRP)-based PL in the proposed $P^2L$ platform. The addition of galactose and phenol derivatives initiates the enzymatic cascade to perform proximity labeling. (C) $P^2L$ enables fast logic computation on the cell surface and the introduction of handles into the microenvironment of the two-level spatially localized biological sites for measurement and manipulation.

From a sensitivity perspective, spatial selectivity should be superimposed in a "catalytic-to-catalytic" manner to progressively amplify the "transferred spatial information". In terms of applicability (e.g., incorporation of post-translational modifications), it is preferable to achieve spatial localization in a non-genetic manner.

Herein, we introduced the galactose oxidase (GAO)-mediated reaction, which catalyzes the oxidation of galactose (Gal) to produce $H_2O_2$,[11] as a regulatory switch and cascaded it upstream of the HRP-based PL reaction. By targeting GAO and HRP to biomarkers indicative of different biological hierarchies (or spatial levels), we developed a two-level spatially localized proximity labeling ($P^2L$) platform (Scheme 1B). In the presence of substrates (Gal & phenol derivatives), the enzyme cascade reaction, catalyzing the covalent attachment of phenol derivatives to the neighboring proteins of HRP, can only take place when the concentration of $H_2O_2$ at the HRP anchor site (generated by the GAO reaction and then diffused) reaches the threshold for activating the PL reaction. Using *cellular*- and *glycan*-level as model hierarchies, we successfully implemented proximity labeling with localization across 2 biological hierarchies in complex cellular systems, confirming that $P^2L$ can efficiently perform 2-step logic computations. The target cells with different glycosylation levels can be distinguished in mixed cell populations using a 2-min labeling reaction (Scheme 1C). We also used $P^2L$ to install bio-orthogonal click-reactive groups in the environment of the given glycans of target cells, thereby directing cell-selective fixed-point intercellular covalent assembly. Finally, by combining proteomics techniques with $P^2L$, the microenvironmental proteome of the target glycans on the surface of tumor cells was selectively obtained in a tumor-immune cell interaction system, contributing to the elucidation of the mechanisms by which tumors respond to immune pressure via the glycan recognition axis.

## Results and Discussion

### Design of Enzyme Reaction Cascade for Proximity Labeling

We first constructed a GAO-HRP cascade on the surface of living cells and verified the feasibility of cascade-based proximity labeling. The enzymatic cascade can be conceptualized as a two-step logic computation with the labeling signal as the output, representing a novel form of logic operation (Figure 1A).

Cholesterol and fluorophores were modified on two enzymes to obtain Chol-GAO-FITC and Chol-HRP–Cy5 (Figure S1), the cholesterol being used to anchor the enzymes to the cell surface and the latter being used to track the anchoring conditions (Figure S2). Using HeLa cells as a model, SA–Cy3 fluorescence was only observed at the cell periphery when both Gal (5 mM) and biotin-phenol (BP, 20 μM) were added (Figure 1B, Figure S3–S4). We then anchored different combinations of enzymes to the surface of HeLa cells (Figure 1C). Only the cells with both GAO and HRP anchored exhibited a labeling signal, demonstrating the feasibility of proximity labeling by sequential activation of two enzymatic reactions. When exogenous $H_2O_2$ was added (Figure S5), cells were labeled as long as they had been anchored with HRP. This situation is equivalent to the usual PL, suggesting that the GAO reaction can be regarded as a logic operation that serves as first-level spatial localization.

The two enzymatic reactions are cascaded relying on the diffusion of $H_2O_2$, and the distribution of the concentration

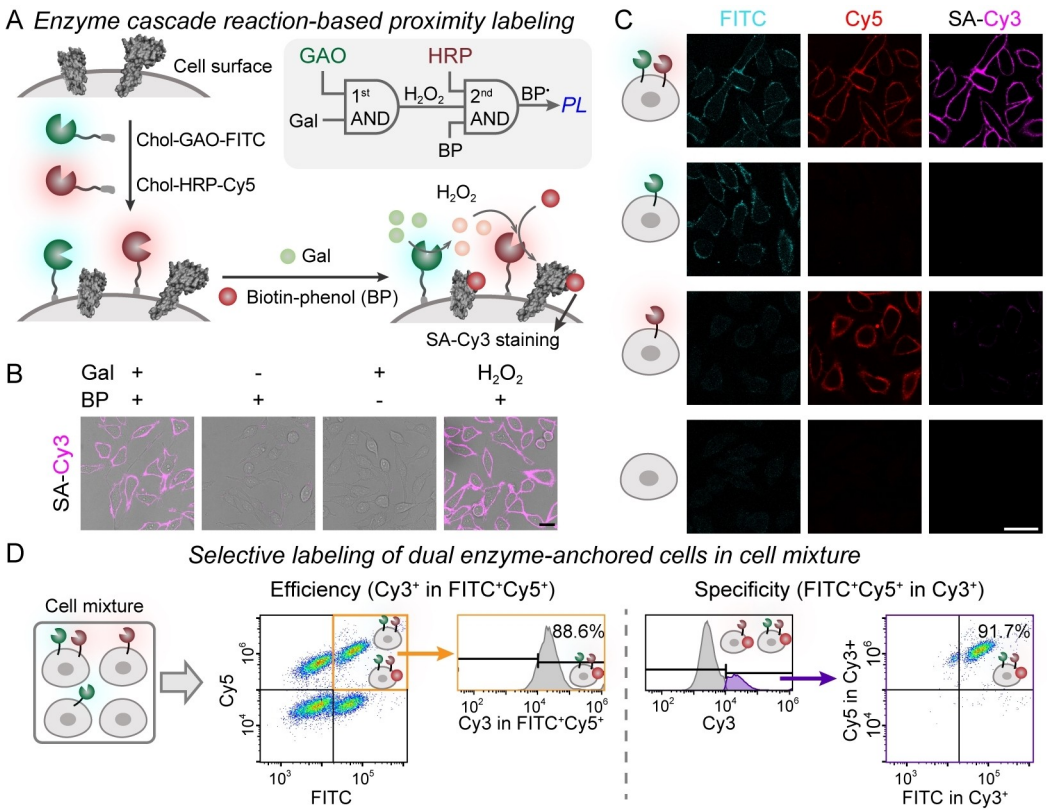


***Figure 1.*** Cascading enzymatic reactions on the cell surface for proximity labeling. (A) Schematic illustration of the installation of cholesterol (Chol) & fluorophore co-modified enzymes on the cell surface to perform proximity labeling, along with the logic operation principle. (B) CLSM images of HeLa cells after dual enzyme anchoring, treatment with different substrate combinations, and SA–Cy3 staining. (C) CLSM images of HeLa cells carrying different enzyme combinations after proximity labeling (Gal + BP) and SA–Cy3 staining. (D) Investigation of labeling efficiency and specificity of dual enzyme-anchored cells ($GAO^+$ & $HRP^+$) in the cell mixture. Cells carrying different enzyme combinations were treated with BP and Gal in the presence of catalase, followed by SA–Cy3 staining and FCM analysis. Scale bars: 25 μm. Data are representative of three independent experiments.

gradient of $H_2O_2$ within the labeling time window determines the area of the 1st spatial localization. We deduced that the minimum concentration of $H_2O_2$ (2 μM) required to initiate the HRP-based reaction within a 1-min labeling period is at a diffusion radius of 9.2 μm (with the GAO site set as the origin) (Figure S6).[12] This radius is smaller than the size of a single mammalian cell and therefore the HRP reaction can be confined to the target cells when cascaded with the GAO reaction.

To confirm this, we mixed four types of cells carrying different enzyme combinations and initiated the labeling process (Figure S7A). The labeling efficiency (percentage of labeled target cells in total target cells) of the dual enzyme-anchored cell group was 97.2 %, while the specificity (percentage of labeled target cells in total labeled cells) was slightly lower (64.3 %), which could be attributed to intercellular $H_2O_2$ diffusion. Either the addition of catalase (CAT, 100 μg/ml) or an increase in BP concentration improved the cell selectivity (Figure 1D, Figure S7A). In particular, the addition of CAT resulted in a labeling efficiency of 86.4 % and an improved specificity of 90.2 % (Figure S7B). These results lay the foundation for the next step of establishing $P^2L$ for molecular measurements across biological hierarchies.

### *Two-Level Spatially Localized Proximity Labeling ($P^2L$) Platform*

We went on to specifically target the two enzymes to markers indicative of two different biological hierarchies to demonstrate the labeling feasibility of the $P^2L$ platform (Figure 2A). The first *cellular* level used mucin 1 (MUC1)-positive HeLa cells (human cervical cancer cell line) and MUC1-negative A549 cells (human lung cancer epithelial-like cell line) as models (Figure S8–S9). The second *glycan* level used $N_3$-modified sialic acids (Sia) as the model, which were constructed by metabolic oligosaccharide engineering (Figure S10).[13] The resulting set of cell samples included: $HeLa^H$ ($MUC1^+$, Sia-$N_3^H$), HeLa ($MUC1^+$, Sia-$N_3^-$), $A549^H$ ($MUC1^-$, Sia-$N_3^H$) and A549 ($MUC1^-$, Sia-$N_3^-$) (Figure S11). H indicates a high modification level of Sia-$N_3$ on the cell.

We chose glycans as the second-tier target because, with the rapid development of glycobiology, there is a broad consensus in the scientific community that "glycosylation

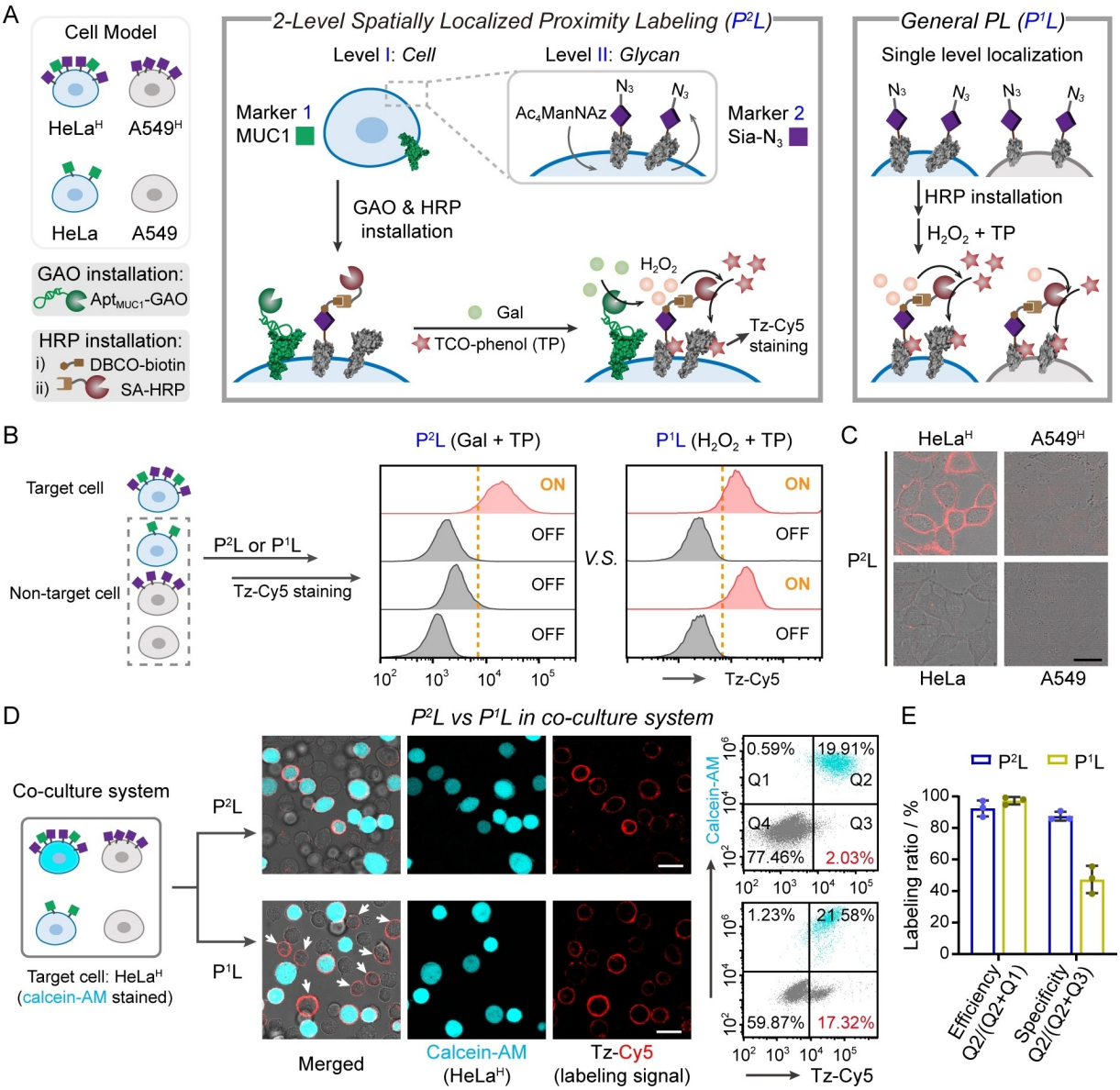


***Figure 2.*** Design of 2-level spatially localized proximity labeling ($P^2L$) platform. (A) Schematic diagram of $P^2L$ and general PL (i.e., $P^1L$). Using MUC1 and Sia-$N_3$ as the markers for the *cellular*- and *glycan*-level spatial localization, respectively, a set of four cell samples was constructed. Sia-$N_3$ is developed by metabolic labeling of Sia with $Ac_4ManNAz$. The $P^2L$ operation involves the installation of GAO and HRP and the Gal-triggered TP labeling; and the $P^1L$ operation involves the HRP installation and the $H_2O_2$-triggered TP labeling. The difference in labeling mechanisms between $P^2L$ and $P^1L$ is shown. (B) Demonstration of the advantage of $P^2L$ over $P^1L$. FCM analysis of the cell set after $P^2L$ or $P^1L$ operation and tetrazine-Cy5 (Tz–Cy5) staining. (C) CLSM images of the cell set after $P^2L$ operation and Tz–Cy5 staining. Scale bar: 25 μm. (D) Comparison of the performance of $P^2L$ and $P^1L$ in co-culture system. CLSM images and FCM data of the co-cultured cell set after different operation ($P^2L$ or $P^1L$) and Tz–Cy5 staining. Target cells ($HeLa^H$) were pre-stained with calcein-AM. White arrows indicate the non-target cells with obvious proximity labeling signal. Scale bars: 25 μm. (E) Labeling efficiency and specificity of the target cells obtained from (D) by calculating Q2/(Q2 + Q1) and Q2/(Q2 + Q3). Data in (B–D) are representative of three independent experiments. Data in (E) are shown as mean ± SD, $n = 3$.

dramatically increases the structural and functional diversity of biological systems".[14] Superimposing the glycan dimension on the protein marker dimension is an encouraging solution for developing novel disease biomarkers, vaccines and targets, overcoming the challenges of drug off-target effects and resistance, and ultimately facilitating personalized treatment.[15] However, because glycans require complex chemical labeling mechanisms[13] that are difficult to incorporate into cellular identification criteria, most biological localization is currently achieved by targeting proteins with little consideration of glycosylation. Our proposed $P^2L$ platform has broad applicability for different localization mechanisms, allowing the incorporation of *cellular* and *glycan* hierarchies into the logic computational framework of cell identity.

We conjugated GAO with an aptamer (SH-$Apt_{MUC1}$) that specifically recognizes MUC1 (Figure S9, Figure S12),[16] and the resulting GAO-$Apt_{MUC1}$ can specifically bind to MUC1-positive cells (Figure S13). Sequential treatment with DBCO-biotin and SA-HRP was used to install HRP on Sia-$N_3$ of metabolically labeled cells (Figure 2A). We then added *trans*-cyclooctene-phenol (TCO-phenol, TP, 200 μM, Figure S14) and Gal (10 mM, Figure S15) to the 4 types of cell models to initiate the $P^2L$ process (Figure 2B–2C, Figure S16A, S17). TP signals were observed exclusively on the $HeLa^H$ cell surface, as indicated by tetrazine-Cy5 (Tz–Cy5) staining, with a mean fluorescence intensity (MFI) ratio of 16.2 compared to HeLa cells. To demonstrate the advantage of $P^2L$, the $P^1L$ procedure with HRP installation on Sia-$N_3$ and $H_2O_2$-triggered TP labeling was also performed on the 4 cell samples by starting the reaction with $H_2O_2$ (10 μM) and TP (200 μM) (Figure 2B, Figure S16B). In this case, however, TP signals were detected on both $HeLa^H$ and $A549^H$ cells, i.e., $P^1L$ could not distinguish between different cells carrying Sia-$N_3$.

We also simultaneously inoculated the four cell populations mentioned above into the same culture well (Figure S18A) and compared the performance of $P^2L$ and $P^1L$. $P^2L$ displayed a significant labeling selectivity compared to $P^1L$ (Figure 2D, Figure S18B–S20), achieving a labeling efficiency of 92.9 % and a specificity of 87.4 % (Figure 2E). These results demonstrate that $P^2L$ successfully achieves proximity labeling with localization across 2 biological hierarchies (from *cellular* down to *glycan* level) through cascading enzymatic reactions.

### *Efficient Cell-Surface Logic Computation Capability of $P^2L$*

The $P^2L$ method, as a logic computational approach, is capable of identifying cell subtypes by sequentially calculating the presence of two biological features (Figure 3A). The characteristics of the catalytic cycle and the diffusion properties of $H_2O_2$ (Figure S6) facilitate the transfer of spatial proximity information between markers 1 and 2. Meanwhile, the HRP-catalyzed PL reaction possesses an intrinsic ability to amplify the signals from marker 2. These two factors provide enzyme cascade-based logic gates with an unrivaled advantage in terms of computation time, running for only 1 to 3 min. In contrast, conventional logic gates constructed based on DNA[17] or proteins[18] typically rely on the physical contact between the probes attached to the targets to initiate the 1:1 type (non-catalytic) logic operations and require the additional introduction of signal amplification techniques to enhance the signals, which generally takes more than 1 h.[19]

To confirm the high sensitivity of $P^2L$, we additionally constructed a $HeLa^L$ model characterized by low expression of Sia-$N_3$ (Figure 3B, Figure S21), with an abundance of 31.2 % of that observed in $HeLa^H$ and 48.5 % of the detectable MUC1 level (Figure S22–S23). For $HeLa^L$, the 1-min labeling operation yielded a fluorescence signal that was 4.5 times that of HeLa (Figure 3C).

This ratio is 27.8 % of that for $HeLa^H$ (Figure 2B), which is consistent with the target abundance ratio and substantiates the cross-hierarchy quantification capability of $P^2L$. Extending the labeling time from 1 to 3 min increased the MFI ratio of $HeLa^L$ to HeLa to 13.2 (Figure 3C). A similar phenomenon was observed on HeLa cells with further reduced Sia-$N_3$ abundance (Figure S24), suggesting that increasing the labeling time by just a few minutes can significantly improve the labeling sensitivity.

We also constructed an $A549^L$ model with low Sia-$N_3$ levels and evaluated the capability of $P^2L$ to identify target cells with low glycosylation levels in mixed cell populations including $HeLa^L$ (target cells), HeLa, $A549^L$, and A549 (Figure S25A). Extending the labeling time resulted in a significant increase in the labeling signal of $HeLa^L$, thereby enhancing the labeling efficiency; however, an increased signal from non-target cells was also observed, leading to a decrease in the labeling specificity. Notably, when the labeling time was set to 2 min, both high labeling efficiency and labeling specificity for $HeLa^L$ were successfully achieved (Figure S25B, C).

Furthermore, we investigated whether $P^2L$ is capable of differentiating target cells with different glycosylation levels by constructing a co-culture system in which $HeLa^H$ and $HeLa^L$ cells were co-cultured with $A549^L$ and A549 cells. Performing $P^2L$ with a 2-min TP labeling proved to be sufficient to sensitively differentiate between $HeLa^H$ and $HeLa^L$ (Figure 3D–F, Figure S26). In general, glycosylation exhibits considerable heterogeneity, often characterized by variations in high or low modification levels (for example, one of the typical features of tumors is hyper-sialylation),[20] making it difficult to use the presence or absence of a single glycan structure as a reliable marker. Our proposed $P^2L$ provides a powerful tool for identifying cells with different glycosylation modifications within complex biological systems.

### *Covalent Intercellular Assembly at $P^2L$-Designated Sites*

The covalent tags generated by $P^2L$ provide robust "handles" for precise programming of cellular interactions within complex systems in a cell- and site-selective manner. To demonstrate this, we used $P^2L$ to introduce TCO at the Sia site of $HeLa^H$ cells (generating TCO-$HeLa^H$) and covalently modified Tz on the surface of Jurkat T cells (generating Tz-Jurkat, Figure S27), to construct a pair of cell models that can be covalently assembled via a click reaction (Figure 4A).[21]

Robust attachment of the "handles" to the cell surface is a prerequisite for efficient manipulation of cell behavior. Therefore, we first investigated the stability of TCO tags on the target cells ($HeLa^H$). After $P^2L$ operation and Tz–Cy5 staining, $HeLa^H$ cells were cultured in either complete or incomplete medium for different time periods, up to 4 h. The retention percentage of TCO on the cell surface exceeded 47 % in both cases, while in the complete medium the percentage was slightly higher, perhaps due to the physical protective effect of the serum on the cells, which may slow down the fluidity of the cell membrane. However, the $Apt_{MUC1}$-TCO (Figure S28) bound to $HeLa^H$ was signifi-

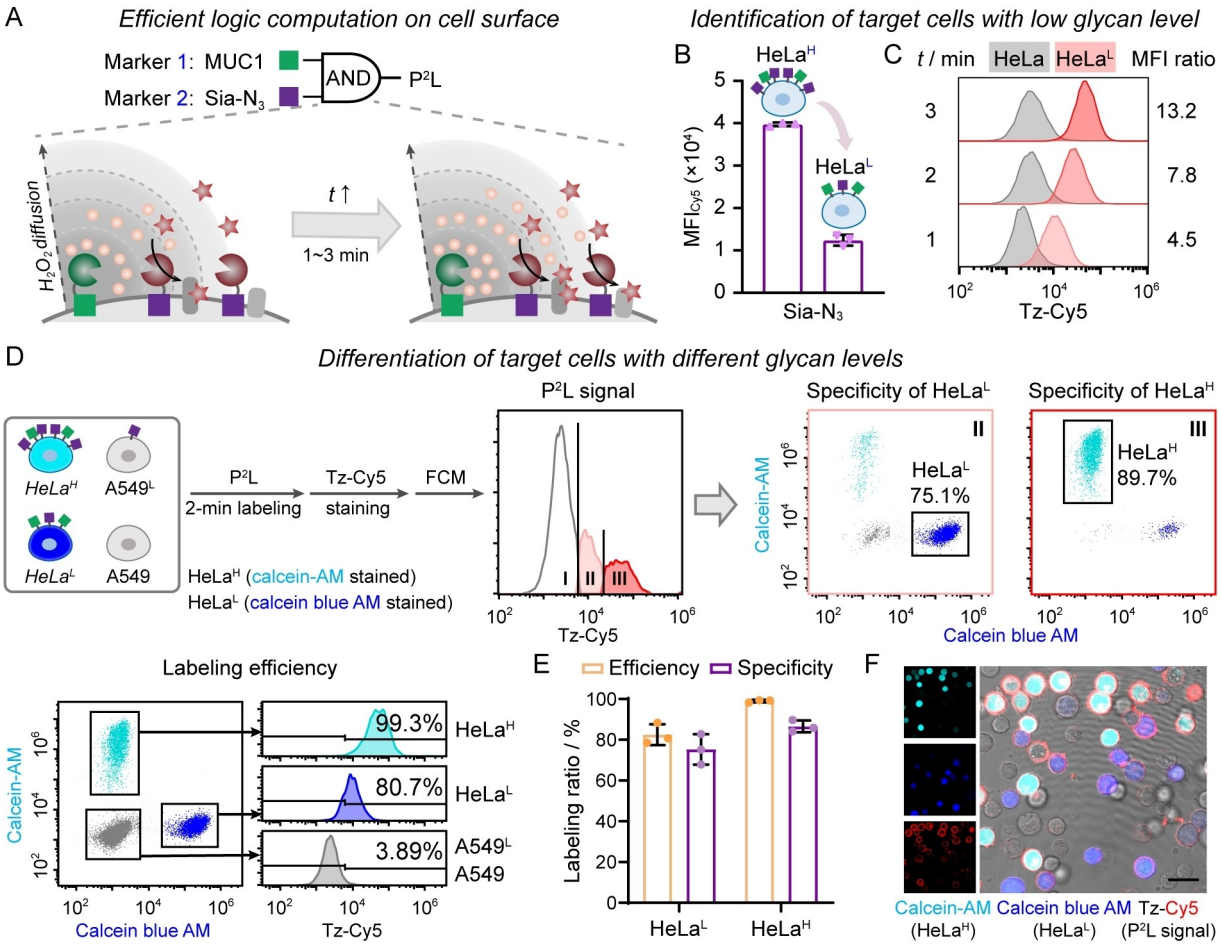


***Figure 3.*** Demonstration of the efficient logic computation capability of P²L on the cell surface. (A) Schematic showing the logic computation principle of P²L. Owing to the fast diffusion of $H_2O_2$ and the signal amplification capabilities of the two enzymes, the P²L-based logic computation can efficiently transfer the localization information and be executed at the minute level. (B) The Sia-$N_3$ levels of HeLa cells undergoing different metabolic labeling treatments ($HeLa^H$ and $HeLa^L$, full data are shown in Figure S21). (C) FCM analysis of $HeLa^L$ after performing P²L with different labeling time, followed by Tz–Cy5 staining. HeLa cells without Sia-$N_3$ were used as a control. The relative MFI ratio of $HeLa^L$ to HeLa is shown. (D) Differentiation of target cells with different glycan levels in the co-culture system analyzed by FCM. The labeling specificity and efficiency of the target cells are shown. Target cells $HeLa^H$ and $HeLa^L$ were stained with calcein-AM and calcein blue AM, respectively. (E) Summary of the labeling efficiency and specificity from (D). (F) CLSM images of the cell mixture from (D). Scale bar: 25 μm. Data in (C, D, F) are representative of three independent experiments. Data in (B, E) are shown as mean ± SD, $n = 3$.

cantly less stable in complete medium (Figure 4B, Figure S29). These data suggest that the covalent tags generated by P²L exhibit enhanced stability.

After incubation of TCO-$HeLa^H$ and Tz-Jurkat cells in a 1:4 ratio at room temperature for 30 min, 23.1 % of the $HeLa^H$ cells were successfully assembled, a percentage significantly higher than that of cells lacking Tz or TCO modifications (Figure S30). When the temperature was raised to 37 °C, the assembly ratio increased to 51.0 % and remained largely unaffected by the presence of fetal bovine serum (FBS) (Figure 4C, D), confirming the stability of covalent cellular assembly under physiological conditions.

Finally, we used P²L in the co-culture system to introduce "handles" to the target cells for cell-selective programming of intercellular interactions. After performing P²L and cell digestion, the cell mixtures were incubated with Tz-Jurkat cells in a 1:1 ratio at 37 °C for 30 min (Figure 4E). The assembly percentage of $HeLa^H$ cells (47.6 %) was significantly higher than that of non-target cells (14.6 %). In the control group without P²L treatment, no significant difference in the assembly percentage was observed (Figure 4F–H, Figure S31). These experiments demonstrated that P²L can designate the assembly site with a two-level spatial localization, extending the application of proximity labeling and providing novel methods for the precise manipulation of cellular interactions for tissue engineering.

### *Tracking Changes in the Microenvironment of Sia*

The tumor microenvironment (TME) is a typical multi-level biological system characterized by the complex networks of interactions between different cell types.[22] One research area of great interest in the TME is the relationship between

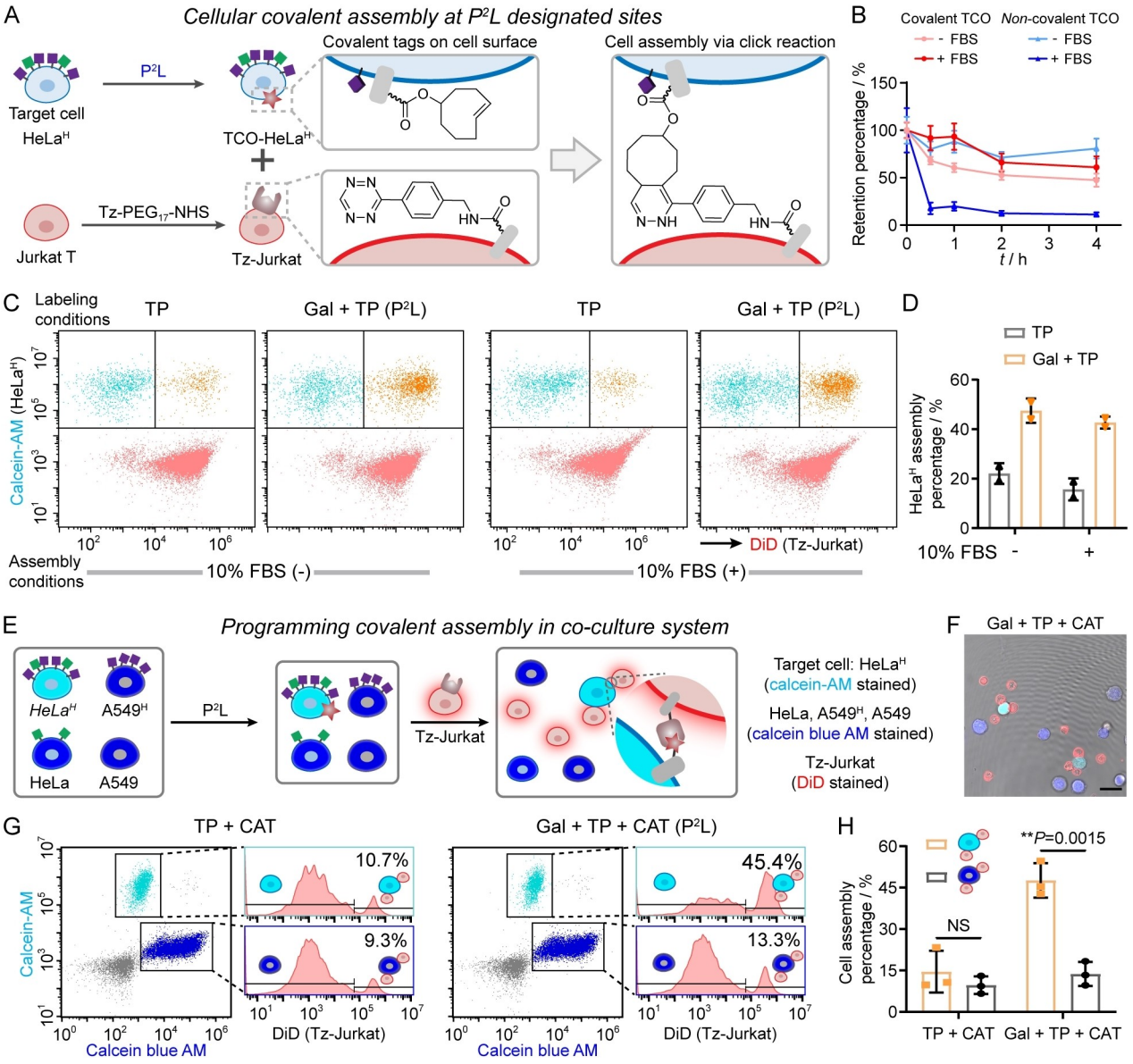


***Figure 4.*** Programming of cellular covalent assembly at P²L-designated sites. (A) Schematic illustration of cell-cell covalent assembly programmed by P²L and bio-orthogonal click reaction. (B) Investigation of the stability of P²L-introduced TCO (covalently linked) on the HeLa$^H$ surface. A control for non-covalent TCO modification was prepared by incubating HeLa$^H$ cells with TCO-modified Apt$_{MUC1}$. The retention percentage of covalent or non-covalent TCO on the cell surface after incubation in the culture medium with or without 10% FBS for different time periods (0, 0.5, 1, 2, 4 h) was recorded. Data are shown as mean ± S.D. of 30 cells from 3 independent experiments. (C) Covalent assembly of TCO-tagged HeLa$^H$ cells and Tz-modified Jurkat T cells. FCM analysis of HeLa$^H$ cells after P²L operation (Gal + TP), followed by incubation with Tz-Jurkat in PBS with or without 10% FBS at 37 °C for 30 min. HeLa$^H$ cells subjected to P²L without the addition of Gal were used as controls. HeLa$^H$ and Tz-Jurkat cells were pre-stained with calcein-AM and DiD, respectively. Data are representative of two independent experiments. (D) HeLa$^H$ cell assembly percentage from (C), which was obtained by dividing the total HeLa$^H$ amount by the amount of HeLa$^H$ with Jurkat T assembled. Data are shown as mean ± SD, $n = 2$. (E–H) Programming of cellular covalent assembly in a co-culture system. (E) Schematic diagram of the assembly procedure. (F) CLSM images and (G) FCM data of co-cultured cells (HeLa$^H$, HeLa, A549$^H$ and A549) after P²L operation (Gal + TP + CAT), followed by incubation with Tz-Jurkat at 37 °C for 30 min. The co-culture system subjected to a similar treatment but without Gal was used as a control. HeLa$^H$ and Tz-Jurkat cells were pre-stained with calcein-AM and DiD respectively, other cells (HeLa, A549 and A549$^H$ cells) were pre-stained with calcein blue AM. Scale bar: 25 μm. (H) Cell assembly percentage from (G). Data in (F) and (G) are representative of three independent experiments, and data in (H) are shown as mean ± SD, $n = 3$. Statistical significance was determined by unpaired two-tailed $t$-test; NS, not significant ($P > 0.05$), $^{**}P \leq 0.005$.

tumor cells and macrophages.[23] In particular, M2-like tumor-associated macrophages have been shown to promote tumor progression by secreting anti-inflammatory factors.[24] A critical aspect of tumor development is the alteration of glycosylation patterns.[25] Investigating the influence of tumor-macrophage interactions on tumor glycosylation and its recognition behavior may provide valuable insights into the evolutionary mechanisms of tumors in response to

immune pressure, particularly from the perspective of glycosylation.

Sia is located at the end of glycan chains and is closely associated with tumor progression.[25] We first investigated the alterations of Sia on the surface of human lung cancer epithelial-like A549 cells in the co-culture system with M2 macrophages (Figure S32). As the co-culture time increased, the Sia level on the surface of A549 cells showed a significant increase when compared to the individual culture model (Figure 5B, C, noted that the effect of exocytotic molecules on click staining reaction was excluded). This finding indicates that the presence of macrophages indeed influences the glycosylation patterns of A549 cells.

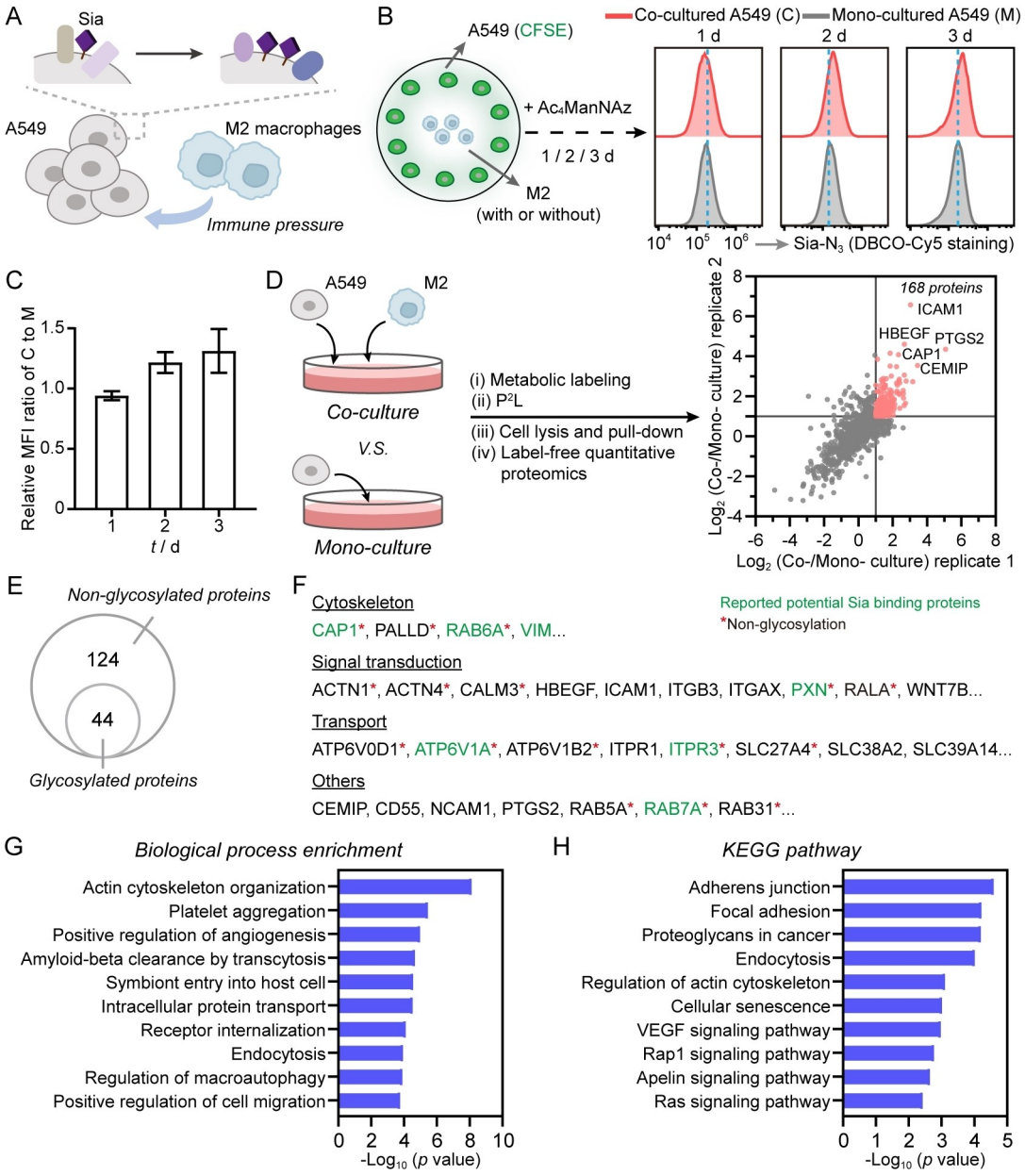


***Figure 5.*** Microenvironment profiling of A549 cell surface Sia in response to macrophage co-culture. (A) Schematic diagram showing the influence of M2 macrophage co-culture on the sialylation level and Sia microenvironment of A549 cells. (B) Experimental design and representative FCM data for tracking the macrophage-induced Sia variation (1–3 d) on A549 cells (*abbr.*, C). DBCO–Cy5 was used to stain the metabolic ($N_3$) labeled Sia. Control: mono-cultured A549 cells (*abbr.*, M). (C) Relative MFI of co-cultured A549 cells normalized to mono-cultured A549 cells. Data in (C) are shown as mean ± SD, $n=2$. (D) Proteomic profiling of the A549 cell surface Sia microenvironment in response to M2 macrophages. Two-dimensional scatter plot of proteins identified and quantified in two independent experiments. Proteins with $Log_2$ (Co-culture/Mono-culture) ratio ≥ 1 in both experiments are highlighted in red and identified as upregulated proteins. The complete list can be found in Dataset S1. (E) Number of identified upregulated proteins with and without glycosylation. (F) Examples of identified upregulated proteins categorized by different functions. Proteins in green are reported potential Sia binding proteins, and those with red asterisks are non-glycosylated proteins. (G) Biological process enrichment and (H) KEGG pathway analysis of the identified upregulated proteins from (D) by DAVID.

Building on this, we sought to integrate $P^2L$ and proteomic technology to elucidate the alterations occurring within the Sia microenvironment. Given that A549 cells and M2 macrophages exhibit positive and negative expression of the hepatocyte growth factor receptor (MET), respectively (Figure S33), we selected MET as the 1st marker, and used the MET aptamer SL1[26] ($Apt_{MET}$, Figure S34) to direct GAO towards A549 cells, achieving the *cellular*-level spatial localization. For the 2nd marker, Sia-$N_3$, we prepared and characterized Tz-modified HRP (Tz-HRP), and used DBCO-TCO to anchor Tz-HRP onto Sia-$N_3$ (Figure S35). The feasibility of $P^2L$ operation was confirmed using 10 mM Gal and 100 μM BP (Figure S36), and the effect of exocytotic $H_2O_2$ on $P^2L$ was excluded.

We conducted $P^2L$ operation on both co-cultured system and mono-cultured A549 cells over a duration of two days, followed by enrichment of biotin-labeled proteins and label-free proteomics analysis (Figure 5D). 168 cell surface proteins were identified to exhibit upregulation in response to immune pressure, with $Log_2$ (Co-culture/Mono-culture) $\geq 1$ (Figure 5D). Uniprot database (www.uniprot.org) queries confirmed that 44 of these identified proteins were glycosylated (Figure 5E). We speculated that these upregulated proteins include the sialylated proteins themselves, their interacting partners, and spatially adjacent proteins (Figure 5F).

Several identified upregulated glycoproteins, including CEMIP (cell migration inducing hyaluronidase 1), ICAM1 (intercellular adhesion molecule 1), HBEGF (proheparin-binding EGF-like growth factor) and PTGS2 (prostaglandin-endoperoxide synthase 2), are closely associated with the adhesion, migration, and invasion of tumor cells. For example, the overexpression of CEMIP is related to poor prognosis in non-small cell lung cancer and may facilitate tumor metastasis by modulating the epithelial-mesenchymal transition (EMT) signaling network.[27] Furthermore, PTGS2 is also overexpressed in lung cancer and plays a critical role in lung carcinogenesis and progression by promoting angiogenesis, metastasis, and immune suppression.[28] Several reported potential Sia binding proteins, such as RAB7 A (Ras-related protein Rab-7a)[29] and PXN (paxillin)[30] were also found. RAB7 A has been shown to regulate the immigration of lung cancer cells through its interaction with Rac1 and vimentin (VIM),[31] and may be involved in the regulation of cell surface Sia.[32] PXN has been reported to enhance the proliferation and invasion of lung cancer cells,[33] and it can be activated through the sialylation of integrin β1.[30]

We then conducted a biological process enrichment analysis and a KEGG pathway analysis on these 168 proteins via DAVID.[34] In addition to commonly recognized glycosylation-related biological processes such as cell migration, angiogenesis, and symbiont entry into host cells, the upregulated proteins are also associated with processes such as protein internalization and endocytosis. This suggests that the increased sialylation observed in tumor cells in the context of immune pressure may play a regulatory role in these related processes (Figure 5G). Furthermore, the KEGG analysis indicates that these proteins are involved in various signaling pathways, including those related to the actin cytoskeleton, focal adhesion, adherens junction, VEGF and Rap1, and are associated with the regulation of cancer cell migration and proliferation (Figure 5H).

These results indicate that the integration of $P^2L$ and proteomic technology has equipped in situ analysis with spatial specificity across two biological hierarchies. This advance allows the unveiling of molecular information about the microenvironment surrounding specific biomolecules on specific cells within heterogeneous cellular systems. As a result, $P^2L$ can serve as a powerful tool for uncovering the molecular mechanisms underlying complex interaction systems.

## Conclusion

In conclusion, to address the current limitations of PL technology, which is limited to single-level spatial localization, we developed a two-level spatially localized proximity labeling ($P^2L$) platform. This platform integrates a GAO-based oxidation reaction (as a temporal and spatial switch) upstream of the HRP-based PL reaction. The $P^2L$ platform effectively transfers and amplifies the spatial localization signal, acting as a logic gate and overcoming the specificity and stability issues associated with biological labeling. The output of covalent tags can be docked with cell assembly programming and microenvironment profiling, thereby providing versatile tools for the analysis and manipulation of complex biological systems.

In comparison to existing research on cell surface logic gates, we incorporated the two biological hierarchies, at the *cellular* and *glycan* levels, into the computational framework of cell identity, and demonstrated the quantitative differentiation capabilities of $P^2L$ using the *glycan* level as a model. Using phenol derivatives with click-reactive groups as substrates, the tags introduced by $P^2L$ exhibited both spatial selectivity and covalent reactivity. This allows the precise programming of cell assembly within complex cellular systems, which holds promise for fine-tuning intercellular interactions, such as assembly sites or intercellular spacing. Using the two-level spatial localization of $P^2L$, we analyzed the microenvironment of Sia on the surface of target cells in co-culture models, establishing a research paradigm to reveal the effects of glycosylation in a spatially selective manner within a complex biological environment.

The $P^2L$ platform is flexible in terms of installation format (affinitive or covalent), making it applicable to different categories and types of markers. This versatility will facilitate the future application of $P^2L$ in the analysis and classification of cancer cells,[35] tumor exocytosis vesicles,[36] and logic operation-guided intelligent immune cell therapeutics,[37] etc. By regulating the labeling time of $P^2L$, the first-level spatial localization scale may be extended and used for the spatial information profiling of proximal and distal cells surrounding the target cells. The spatial information transfer module (enzyme cascade reaction) of $P^2L$ can be designed to operate in other modes. For example, by substituting the two computation units with

light-controlled switches (such as upconversion nanoparticles, UCNPs)[38] and photocatalysts (e.g., $[Ir(dFCF_3ppy)_2(dtbbpy)]PF_6$ and Eosin Y),[39] and by replacing the phenol substrate with diazirine (a photocatalytic substrate with a smaller labeling radius), the proximity labeling region can be further focused (~10 nm),[40] and the in vivo use of $P^2L$ can be expected.

## Supporting Information

The authors have cited additional references within the Supporting Information.[3j,12, 41]

## Acknowledgements

We gratefully acknowledge support from the National Natural Science Foundation of China (22274073).

## Conflict of Interest

The authors declare no conflict of interest.

## Data Availability Statement

The data that support the findings of this study are available from the corresponding author upon reasonable request.

**Keywords:** Cellular assembly · Enzymatic cascade · Logic computation · Proximity labeling · Two-level spatial localization

[1] S. F. Banani, H. O. Lee, A. A. Hyman, M. K. Rosen, *Nat. Rev. Mol. Cell Biol.* **2017**, *18*, 285.

[2] B. Belardi, S. Son, J. H. Felce, M. L. Dustin, D. A. Fletcher, *Nat. Rev. Mol. Cell Biol.* **2020**, *21*, 750.

[3] a) H. W. Rhee, P. Zou, N. D. Udeshi, J. D. Martell, V. K. Mootha, S. A. Carr, A. Y. Ting, *Science* **2013**, *339*, 1328; b) K. J. Roux, D. I. Kim, M. Raida, B. Burke, *J. Cell Biol.* **2012**, *196*, 801; c) T. C. Branon, J. A. Bosch, A. D. Sanchez, N. D. Udeshi, T. Svinkina, S. A. Carr, J. L. Feldman, N. Perrimon, A. Y. Ting, *Nat. Biotechnol.* **2018**, *36*, 880; d) M. Ramanathan, K. Majzoub, D. S. Rao, P. H. Neela, B. J. Zarnegar, S. Mondal, J. G. Roth, H. Gai, J. R. Kovalski, Z. Siprashvili, T. D. Palmer, J. E. Carette, P. A. Khavari, *Nat. Methods* **2018**, *15*, 207; e) K. Kido, S. Yamanaka, S. Nakano, K. Motani, S. Shinohara, A. Nozawa, H. Kosako, S. Ito, T. Sawasaki, *eLife* **2020**, *9*, e54983; f) B. S. Johnson, L. Chafin, D. Farkas, J. Adair, A. Elhance, L. Farkas, J. S. Bednash, J. D. Londino, *Mol. Cell. Proteomics* **2022**, *21*, 1535; g) X. Zhang, Q. Tang, J. Sun, Y. Guo, S. Zhang, S. Liang, P. Dai, X. Chen, *Sci. Adv.* **2023**, *9*, eadg6388; h) E. Joeh, T. O'Leary, W. Li, R. Hawkins, J. R. Hung, C. G. Parker, M. L. Huang, *Proc. Natl. Acad. Sci. USA* **2020**, *117*, 27329; i) H. Zhu, J. H. Oh, Y. Matsuda, T. Mino, M. Ishikawa, Hi. Nakamura, M. Tsujikawa, H. Nonaka, I. Hamachi, *J. Am. Chem. Soc.* **2024**, *146*, 7515; j) Y. Guo, N. Wang, Y. Zhong, W. Li, Y. Li, G. Wang, Y. Yao, Y. Shi, L. Chen, X. Wang, L. Ding, H. Ju, *J. Am. Chem. Soc.* **2023**, *145*, 5092; k) W. Qin, K. F. Cho, P. E. Cavanagh, A. Y. Ting, *Nat. Methods* **2021**, *18*, 133; l) Q. Liu, J. Zheng, W. Sun, Y. Huo, L. Zhang, P. Hao, H. Wang, M. Zhuang, *Nat. Methods* **2018**, *15*, 715; m) Z. Zhang, Y. Wang, W. Lu, X. Wang, H. Guo, X. Pan, Z. Liu, Z. Wu, W. Qin, *bioRxiv preprint* **2024**, DOI: 10.1101/2024.08.22.609124.

[4] a) J. B. Geri, J. V. Oakley, T. Reyes-Robles, T. Wang, S. J. McCarver, C. H. White, F. P. Rodriguez-Rivera, D. L. Jr. Parker, E. C. Hett, O. O. Fadeyi, R. C. Oslund, D. W. C. MacMillan, *Science* **2020**, *367*, 1091; b) Y. Fang, P. Zou, *ChemBioChem* **2023**, *24*, e202200745; c) M. Takato, S. Sakamoto, H. Nonaka, F. Y. T. Valor, T. Tamura, I. Hamachi, *Nat. Chem. Biol.* accepted, DOI: 10.1038/s41589-024-01692-4; d) N. Hananya, X. Ye, S. Koren, T. W. Muir, *Proc. Natl. Acad. Sci. USA* **2023**, *120*, e2219339120; e) D. C. Cabanero, S. K. Kariofillis, A. C. Johns, J. Kim, J. Ni, S. Park, D. L. Parker, Jr., C. P. Ramil, X. Roy, N. H. Shah, T. Rovis, *J. Am. Chem. Soc.* **2024**, *146*, 1337; f) Z. Liu, X. Xie, Z. Huang, F. Lin, S. Liu, Z. Chen, S. Qin, X. Fan, P. R. Chen, *Chem* **2022**, *8*, 2179; g) A. N. Ogorek, X. Zhou, J. D. Martell, *J. Am. Chem. Soc.* **2023**, *145*, 16913; h) Z. Liu, F. Guo, Y. Zhu, S. Qin, Y. Hou, H. Guo, F. Lin, P. R. Chen, X. Fan, *Nat. Commun.* **2024**, *15*, 2712.

[5] J. Li, S. Han, H. Li, N. D. Udeshi, T. Svinkina, D. R. Mani, C. Xu, R. Guajardo, Q. Xie, T. Li, D. J. Luginbuhl, B. Wu, C. N. McLaughlin, A. Xie, P. Kaewsapsak, S. R. Quake, S. A. Carr, A. Y. Ting, L. Luo, *Cell* **2020**, *180*, 373.

[6] S. S. Lam, J. D. Martell, K. J. Kamer, T. J. Deerinck, M. H. Ellisman, V. K. Mootha, A. Y. Ting, *Nat. Methods* **2015**, *12*, 51.

[7] N. D. Udeshi, K. Pedram, T. Svinkina, S. Fereshetian, S. A. Myers, O. Aygun, K. Krug, K. Clauser, D. Ryan, T. Ast, V. K. Mootha, A. Y. Ting, S. A. Carr, *Nat. Methods* **2017**, *14*, 1167.

[8] T. Dang, J. Yu, Z. Cao, B. Zhang, S. Li, Y. Xin, L. Yang, R. Lou, M. Zhuang, W. Shui, *Nat. Chem. Biol.*, accepted, DOI: 10.1038/s41589-024-01714-1.

[9] K. Li, A. Chatterjee, C. Qian, K. Lagree, Y. Wang, C. A. Becker, M. R. Freeman, R. Murali, W. Yang, D. M. Underhill, *Nature* **2024**, *630*, 736.

[10] S. Zhang, Q. Tang, X. Zhang, X. Chen, *ACS Cent. Sci.* **2024**, *10*, 1135.

[11] J. B. Rannes, A. Ioannou, S. C. Willies, G. Grogan, C. Behrens, S. L. Flitsch, N. J. Turner, *J. Am. Chem. Soc.* **2011**, *133*, 8436.

[12] J. Fu, M. Liu, Y. Liu, N. W. Woodbury, H. Yan, *J. Am. Chem. Soc.* **2012**, *134*, 5516.

[13] K. K. Palaniappan, C. R. Bertozzi, *Chem. Rev.* **2016**, *116*, 14277.

[14] C. Reily, T. J. Stewart, M. B. Renfrow, J. Novak, *Nat. Rev. Nephrol.* **2019**, *15*, 346.

[15] S. Mereiter, M. Balmaña, D. Campos, J. Gomes, C. A. Reis, *Cancer Cell* **2019**, *36*, 6.

[16] C. Ferreira, C. Matthews, S. Missailidis, *Tumor Biol.* **2006**, *27*, 289.

[17] L. Chen, W. Chen, G. Liu, J. Li, C. Lu, J. Li, W. Tan, H. Yang, *Chem. Soc. Rev.* **2021**, *50*, 12551.

[18] M. J. Lajoie, S. E. Boyken, A. I. Salter, J. Bruffey, A. Rajan, R. A. Langan, A. Olshefsky, V. Muhunthan, M. J. Bick, M. Gewe, A. Quijano-Rubio, J. Johnson, G. Lenz, A. Nguyen, S. Pun, C. E. Correnti, S. R. Riddell, D. Baker, *Science* **2020**, *369*, 1637.

[19] Q. Gao, Y. Zhao, K. Xu, C. Zhang, Q. Ma, L. Qi, D. Chao, T. Zheng, L. Yang, Y. Miao, D. Han, *Angew. Chem. Int. Ed.* **2020**, *59*, 23564.

[20] C. Büll, M. A. Stoel, M. H. d. Brok, G. J. Adema, *Cancer Res.* **2014**, *74*, 3199.

[21] a) J. C. Jewetta, C. R. Bertozzi, *Chem. Soc. Rev.* **2010**, *39*, 1272; b) H. Koo, M. Choi, E. Kim, S. K. Hahn, R. Weissleder, S. H. Yun, *Small* **2015**, *11*, 6458.

[22] D. Bayik, J. D. Lathia, *Nat. Rev. Cancer* **2021**, *21*, 526.

[23] a) A. Mantovani, P. Allavena, F. Marchesi, C. Garlanda, *Nat. Rev. Drug Discovery* **2022**, *21*, 799; b) D. J. Kloosterman, L. Akkari, *Cell* **2023**, *186*, 13.
[24] I. Vitale, G. Manic, L. M. Coussens, G. Kroemer, L. Galluzzi, *Cell Metab.* **2019**, *30*, 36.
[25] S. S. Pinho, C. A. Reis, *Nat. Rev. Cancer* **2015**, *15*, 540.
[26] R. Ueki, S. Sando, *Chem. Commun.* **2014**, *50*, 13131.
[27] a) F. Deng, J. Lei, X. Zhang, W. Huang, Y. Li, D. Wu, *J. Cancer Res. Ther.* **2017**, *13*, 664; b) Z. Tang, Y. Ding, Q. Shen, C. Zhang, J. Li, M. Nazar, Y. Wang, X. Zhou, J. Huang, *J. Mol. Med.* **2019**, *97*, 127.
[28] a) M. Huang, M. Stolina, S. Sharma, J. T. Mao, L. Zhu, P. W. Miller, J. Wollman, H. Herschman, S. M. Dubinett, *Cancer Res.* **1998**, *58*, 1208; b) T. Hida, K. Kozaki, H. Muramatsu, A. Masuda, S. Shimizu, T. Mitsudomi, T. Sugiura, M. Ogawa, T. Takahashi, *Clin. Cancer Res.* **2000**, *6*, 2006; c) M. Dohadwala, J. Luo, L. Zhu, Y. Lin, G. J. Dougherty, S. Sharma, M. Huang, M. Põld, R. K. Batra, S. M. Dubinett, *J. Biol. Chem.* **2001**, *276*, 20809.
[29] Q. Li, Y. Xie, G. Xu, C. B. Lebrilla, *Chem. Sci.* **2019**, *10*, 6199.
[30] M. Lee, J. Park, Y. Lee, *Oncol. Rep.* **2010**, *23*, 757.
[31] A. Margiotta, C. Progida, O. Bakke, C. Bucci, *Biochim. Biophys. Acta Mol. Cell Res.* **2017**, *1864*, 367.
[32] E. C. Seales, G. A. Jurado, A. Singhal, S. L. Bellis, *Oncogene* **2003**, *22*, 7137.
[33] R. Jagadeeswaran, H. Surawska, S. Krishnaswamy, V. Janamanchi, A. C. Mackinnon, T. Y. Seiwert, S. Loganathan, R. Kanteti, T. Reichman, V. Nallasura, S. Schwartz, L. Faoro, Y. Wang, L. Girard, M. S. Tretiakova, S. Ahmed, O. Zumba, L. Soulii, V. P. Bindokas, L. L. Szeto, G. J. Gordon, R. Bueno, D. Sugarbaker, M. W. Lingen, M. Sattler, T. Krausz, W. Vigneswaran, V. Natarajan, J. Minna, E. E. Vokes, M. K. Ferguson, A. N. Husain, R. Salgia, *Cancer Res.* **2008**, *68*, 132.
[34] D. W. Huang, B. T. Sherman, R. A. Lempicki, *Nat. Protoc.* **2009**, *4*, 44.
[35] Y. Yin, W. Xie, M. Xiong, Y. Gao, Q. Liu, D. Han, G. Ke, X. Zhang, *Angew. Chem. Int. Ed.* **2023**, *62*, e202309837.
[36] J. Deng, S. Zhao, J. Li, Y. Cheng, C. Liu, Z. Liu, L. Li, F. Tian, B. Dai, J. Sun, *Angew. Chem. Int. Ed.* **2022**, *61*, e202207037.
[37] G. M. Allen, W. A. Lim, *Nat. Rev. Cancer* **2022**, *22*, 693.
[38] N. Wu, L. Bao, L. Ding, H. Ju, *Angew. Chem. Int. Ed.* **2016**, *55*, 5220.
[39] a) C. P. Seath, A. J. Burton, X. Sun, G. Lee, R. E. Kleiner, D. W. C. MacMillan, T. W. Muir, *Nature* **2023**, *616*, 574; b) Z. Lin, K. Schaefer, I. Lui, Z. Yao, A. Fossati, D. L. Swaney, A. Palar, A. Sali, J. A. Wells, *Science* **2024**, *385*, eadl5763.
[40] J. V. Oakleya, B. F. Buksha, D. F. Fernandez, D. G. Oblinskyb, C. P. Seatha, J. B. Geria, G. D. Scholesb, D. W. C. MacMillan, *Proc. Natl. Acad. Sci. USA* **2022**, *119*, e2203027119.
[41] H. Cho, H. Kwon, S. H. Lee, H. Lee, N. Kang, Y. Chang, *J. Am. Chem. Soc.* **2023**, *145*, 2951.

Manuscript received: November 4, 2024
Accepted manuscript online: January 13, 2025
Version of record online: ■■, ■■

# Research Article

*Proximity Labeling*

L. Chen, Y. Li, Y. Guo, G. Wang, N. Feng, J. Sun, Y. Zhong, Y. Yao, L. Ding,* H. Ju **e202421448**

Two-Level Spatially Localized Proximity Labeling for Cross-Biological-Hierarchy Measurement and Manipulation

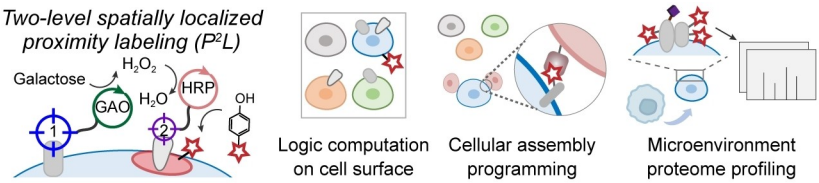


We propose a "two-level spatially localized proximity labeling ($P^2L$)" platform by cascading galactose oxidase (GAO)-based oxidation reaction and horseradish peroxidase (HRP)-based proximity labeling (PL). $P^2L$ integrates enzymatic logic computation and PL, enabling rapid output of spatial localization information across biological hierarchies as covalent tags for cell-selective assembly programming and microenvironmental proteomic analysis.